Velocity of irregular particles continuously avalanching surface flow within rotating drum

S. H. Lin [a], H. Yang[ab], R. Li[a], G. Zheng[c],V. Zivkovic[d]

a. School of Optical-Electrical and Computer Engineering, University of Shanghai for Science and Technology, Shanghai, 200093, China

b. Shanghai Key Lab of Modern Optical System, and Engineering Research Center of Optical Instrument and System, Ministry of Education , University of Shanghai for Science and Technology, Shanghai 200093, China

c. School of Medical instrument and food engineering, University of Shanghai for Science and Technology, Shanghai, 200093, China

d. School of Chemical Engineering and Advanced Materials, Newcastle University, NE1 7RU, United Kingdom

Abstract

Velocity of irregular particles is difficult to measure and analyze due to their irregular shape. A method of spatial filtering velocimetry is used to measure the velocity of particles on the surface of the rotating drum in the rolling mode. The image of the particle flow also shows that the surface is not a straight line but mound exists due to the accumulation of particles at the middle of the drum which influence the velocity profile. The variation of the velocity distribution of irregular particles with drum speeds, particle sizes, and drum diameters is presented and discussed in the paper. The results indicate that there were two velocity peaks in the velocity profile of irregular glass sand at a relatively lower rotating speed. Furthermore, with the increase of the drum speed, the middle valley in the profile gradually moves to the upper right and merges with the second velocity peak and there is only one peak in the velocity profile along streamwise direction of the bed surface consequently similar to spherical particles velocity profile.

1. Introduction

Granular materials display a variety of behaviors that are in many ways different from those of other substances. They cannot be easily classified as either solids or liquids [1]. Granular materials are large agglomeration of distinctive solid particles. When subjected to sufficient external forces, the granular materials exhibit a liquid like flow behavior. Granular materials are widely used in chemical, mineral, ceramic, pharmaceutical and food processing fields, but also plays critical roles in some forms of natural disasters, such as avalanches or landslides [1-5]. Rotating drums are commonly used to process particulate materials in mixing, calcination, granulation and drying operations [4]. With the rotational speed increase, the particle movement in the drum can be classified into six modes: sliding, surging, slumping, rolling, cascading, cataracting and centrifuging regime [5]. The rotating drums are usually operated in rolling regime since it provides superior particle mixing and consequently heat and mass transfer characteristics. This regime is characterized by two regions: active layer and so-called passive layer but the mixing process, heat and mass transfers mainly occur in the active layer [6-8].

Most of the experimental studies are concentrated on the spherical particles, while the studies on irregular particles are less common. At higher rotational speeds, the periodic slumping of the bed gives way to rolling, which is characterized by the continuous motion of a layer of solids over the bed surface [9, 10]. In rolling regime, Khakhar [11, 12] holds that the velocity of spherical particles on surface of avalanching layer is symmetrical. Ding [6] found that at low rotational speed, the velocity

field of spherical particles was approximately symmetric at midpoint, but tends to be skewed at higher rotational speed. Norouzi [13] and Dubé et al. [14] found that spherical and non-spherical particles in the drum surface accelerate first and reach their peak velocity after the mid-chord, after which, particles decelerate. The simulation study of non-spherical particles performed by Suzzi et al. [15] also found the same trend. Longo and Lamberti [16] studied the velocity distribution of glass beads and sand grains in the inner wall of the cylinder, in the midsection, the granular stream is non-accelerated, whereas in the upper and in the lower sections the stream accelerates and decelerates, respectively. Henein [9] confirmed that compared with spherical particles, irregular particle transition to rolling requires higher speed and Froude number; moreover, the static angle of repose of irregular granules is larger than for spherical granules, which is also mentioned in [14,17]. Boateng and Barr [18] found the difference of velocity field between irregular grains and limestone and spherical particle with two or more velocity peaks formed on the bed surface for irregular particles in contrast to the single peaks for spherical particles. Yang [19] found a formation of the small mound at the centre of the avalanching surface using irregular glass sand grains, which was not observed for spherical glass particles. Whether this small mound of irregular particles exists in the rolling mode has not yet been reported. The mound formation obviously can influence the velocity profile on the surface of the bed which is very important boundary for all transport process in the rotating drum []. For example, the velocity profile at the bed surface is used for design of granulation and pan coater equipment as it directly determines the surface residence time which is the time spent by particles on the surface [13, 17]. Furthermore, this velocity profile also is required to determine the residence time in the active layer [14] which mainly controls all transport processes in the drum as outlined above.

There are many techniques for the non-invasive measurements of granular flow velocities [21-29], including Particle Image/Tracking Velocimetry (PIV/ PTV), Laser Doppler velocimetry (LDV), Laser Speckle velocimetry (LSV) and other tomographic methods like Positron Emission Particle Tracking (PEPT) or Magnetic Resonance Imaging (MRI). Among them PIV/ PTV is the most widely used one for the dense granular flow velocity measurement [21-24]. However, PTV requires that each particle can be distinguished clearly which puts huge demand on image resolution and more importantly computing power. While in case of PIV there is no requirement to distinguish each particle, large signal-to-noise of recorded images is desirable requiring for example uniform illumination, which is difficult to obtain due to complex interaction of imaging and lighting system with the observed granular flow, and accompanying experimental set-up [20]. LDV is another widely used method for the measurement of solid or fluid velocities with tracer particles [21]. Once again due to high concentration of the particles and resulting strong light scattering it is not suitable for the dense granular flow with only occasional applications. LSV has been introduced recently for study of surface granular flow due to very good spatial and temporal resolution [19 24, 25]. The limitation is that only velocity fluctuation of particles can be measured, but not the actual particle velocities. Finally, the tomographic methods are typically very expensive and limited to small scale fluidized beds with tracer particle [28, 29].

The spatial filtering velocimetry (SFV) technique, proposed by the Ator in 1963 [30] and improved by Uddin et al. with linear CCD in 1998 [31], has the advantages of low cost, simply and stable structure, and almost universal applicability to all the light reflecting objects. Aizu [32] used the SFV technique to measure the flow velocity of liquid in a capillary glass tube. Xu et al. used an electrostatic sensor array as a spatial filter to measure the velocity of gas-solid two-phase flow particles in the pipeline [33, 34]. Recently, we have tested the suitability of SFV to the measurement of the particles velocities of the surface granular flow in a rotating drum [27].

In this study, we further study the velocity distribution of irregular sand particles on the surface

of rotating drum by linear CCD SFV. After a section on the experimental setup and methods, we first report in the results and discussion section the visual observation of the profile image along with the raw image of SFV. The main part of the results and discussion section includes presentation and discussion on variation of velocity distribution with drum speeds, particle sizes, and drum diameters.

2 EXPERIMENTAL METHOD

2.1 Principle of SFV

Spatial filtering velocity is an optical measurement method using the light scattering of moving objects. The basic operation of this velocimetry is to observe the optical image of a moving object through the spatial filter. Figure 1 shows a schematic of a traditional SFV comprising of an objective lens, transmission grating, focusing lens, and photoelectric sensor. The light is scattered from an object which is moving with velocity v. The scattered light of the moving object is focused on a grating that has spatially periodic transmittance perpendicular to the moving direction of the object. The light passing through the transmission grating is received by a photoelectric sensor. Because of the motion of the moving object, the detected light intensity signal is a temporally periodic signal. The frequency f of this periodic signal contains the information related to the velocity of the object. The relationship between the moving surface velocity v and frequency f is given by following equation [32]

$$v = \frac{pf}{M} \qquad (1)$$

where p is the spatial period of the spatial filter and M is the magnification of the optical system.

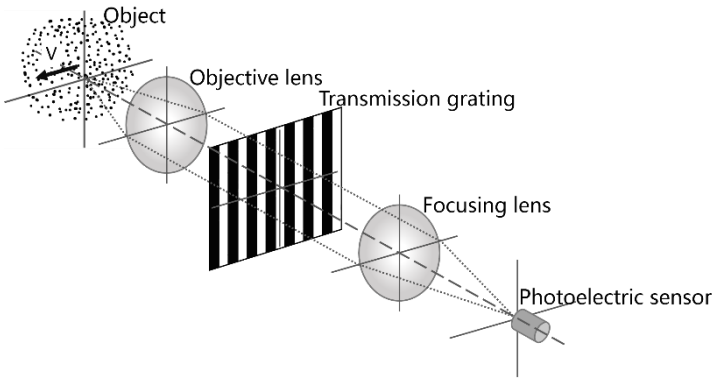

Figure.1 Schematic of spatial filtering velocimetry

The SFV method has the advantages of simple optical system, stable structure and use of non-coherent light source. A linear CCD camera is used as a photoelectric detector and a spatial filter, the optical system of SFV is simplified. Furthermore, the filter composed of physical gratings requires high installation precision, but the linear array CCD solves this problem [35].

Figure 2 shows schematic of spatial filter simulated by linear CCD. The pixels of the linear array CCD are divided into odd parts (white parts) and even parts (black parts) equivalent to the spatial filters S_w and S_g on the structure, respectively. Each part has b pixels, the spatial period, p, is equal to $2b$ pixels.

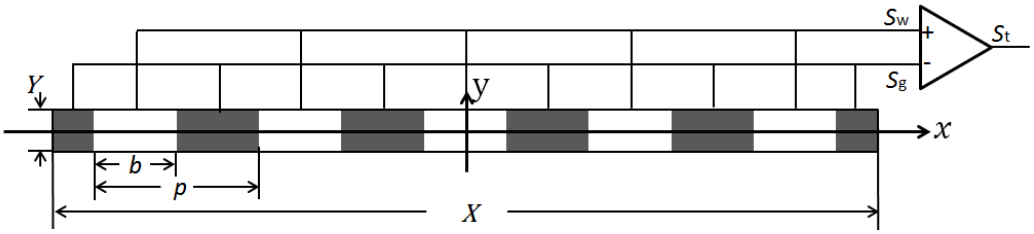

Figure.2 Schematic of spatial filter simulated by linear CCD

The output of space filter S_w and S_g are

$$S_w = \sum_{i=1}^{n} w_i \tag{2}$$

$$S_g = \sum_{i=1}^{n} g_i \tag{3}$$

The spatial filter S_w and S_g can form into a differential spatial filter S_t (i.e. $S_t = S_w - S_g$),which can greatly eliminate the residual signal of the base component because of the non-uniform illumination and low SNR of the output signal, as well as other factors [27]. The central frequency of the differential signal, can be obtained by the fast Fourier transform:

$$S_k = \left| \sum_{t=0}^{N-1} S_t \exp(-j2\pi kt/N) \right| \tag{4}$$

Where S_t is the time-domain signal and N is the FFT point $k = -N, -N+1 \ldots, N-1$.

Figure 3 shows an example of frequency spectrum of the signal from particle system. A frequency spectrum correction algorithm called average-energy barycentre correction is used to obtain the central frequency of the signal shown as smoothed line in the figure. The more details of the average-energy barycentre correction can be found in our recent paper [27]

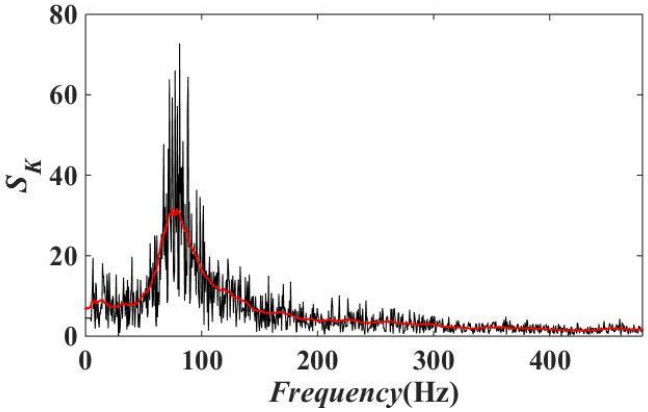

Figure.3 Example of frequency spectrum of the signal from particle system. The red solid line is the result of the average-energy barycentre correction

2.2 Experimental setup

Figure 4 shows the schematic diagram and the image of the experimental setup with the SFV measurement system. The experimental system includes a cylindrical drum, which is made of transparent plexiglass with an inner diameter and a length of 142 mm and 200 mm respectively. The drum, installed on a high precision DC motor platform, is 35% filled with granular materials. The granular material considered in the study are the sieved spherical glass bead particles with size of 0.4

- 0.6 mm and two irregular glass sand particles with size of 0.4 - 0.6 mm (particle A) and 1 - 1.5 mm (particle B) as used in our previous studies [19]. The irregular sand particles are classified as subangular particles with the equivalent projected area diameter (d^{EQPC}) of 1.30 ± 0.17 mm with corresponding sphericity of around 0.87, aspect ratio of 0.69 and convexity of 0.96 based on image analysis. The more detail on the particle properties and image analysis used can be found in our previous paper [19].

The SVS setup are composed of the light source (*i.e.* white LED) and detector (*i.e.* linear CCD camera). The linear CCD camera with optical lens are mounted on the bracket, and the shooting angle of the CCD is adjusted to be perpendicular to the particle flow surface. In our experiment, the surface of the granular materials was not completely flat. If the surface of the sensor is not absolutely parallel to the moving surface, assume that the disturbance angle is θ, the difference of the velocity direction of the moving surface and the linear CCD pixels array, then the measurement velocity is $v'=v\cdot\cos\theta$. Thus, the measurement error is $\Delta v=v\cdot(1-\cos\theta)$. In our case the angle difference is not more than 10°, thus the systematic error of measurement results is no more than 1.5%, which is acceptable in the measurement as the validation study with conveyor belt has error within 3% (average 1.5%) in our previous paper [27]. As figure 4 shows, the measuring range is a very narrow area of the surface of the particle bad, from the top of the surface to the bottom in the middle of the cylinder. In this study, the specification of the linear array CCD is 1024*1, and the sampling frequency is set to 1000 Hz, transmitting the image to the computer through an Ethernet interface. A single lens reflex (Nikon AF 35mm f/ 2D) is used to focus the image of the particles.

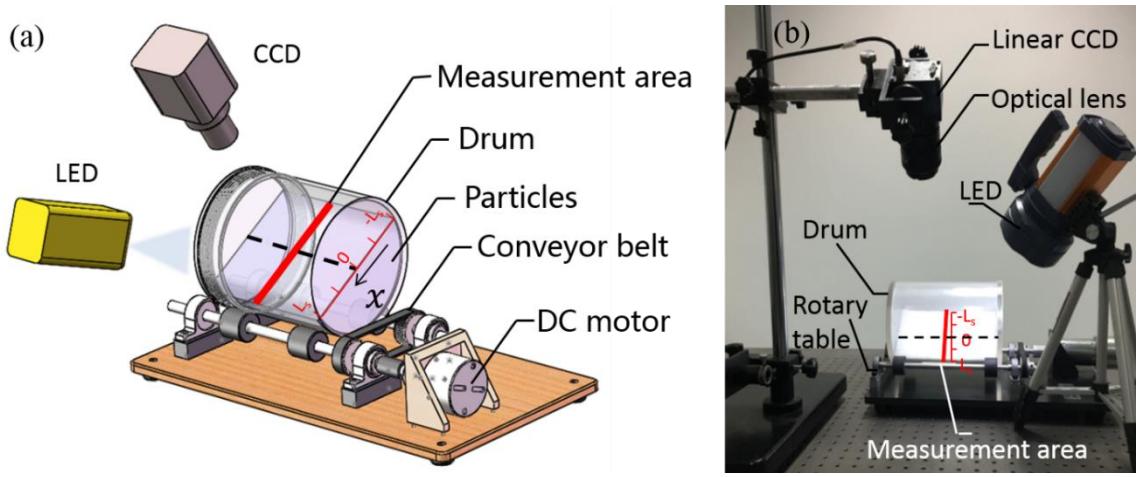

Figure.4 Particle velocity measurement system based on linear CCD SFV.
(a) Schematic diagram and (b) image of experimental setup.

2.3 SFV measurements of spherical particles

Typical results from the measurement of spherical particles are given in Figure 5. Subfigure 5 (a) is a profile image of the drum showing the particle flow surface is flat for the spherical particles when the drum is in rolling state. Figure 5(b) shows composite images of spherical particles from linear array CCD camera with 1024 pixels shown in the X axis while Y axis represent time by the fact the images are stacked one over the other in chronological order. The direction of the X axis is the same as the streamwise motion of the particles. The light streaks in the composite images are the reflected light of different particles, shown in each frame as a different light spot. Thus, these light streaks indicate the motion of the particle across the sequence of multi-frame images, but SFV analysis can provide much more details

Figure 5(c) shows the spherical particle velocity distribution in the x-direction of the drum coming from SFV analysis of the raw images. It can be seen that the maximum velocity of the

spherical particles is located at the center of the particle flow, and the bed surface velocity profile is approximately symmetrical with respect to the mid-chord position in agreement with previous experimental studies [11]. According to Khakhar [11], the streamwise velocity along the bed surface V(x) has the following relationship with maximum velocity V_m(x)

$$\mathrm{V(x)} = V_m(1 - \frac{x^2}{L_s^2}) \tag{5}$$

where the distance L_S, shown in Figure. 4(a). For ease of description, we set-up the position of zero $(\frac{\mathrm{x}}{L_s} = 0)$ at the mid-chord. The fitted lines for spherical particle velocity profile using Eq. 5 are shown in Figure 5(c). This confirms that SFV technique is applicable in measuring streamwise velocity profiles.

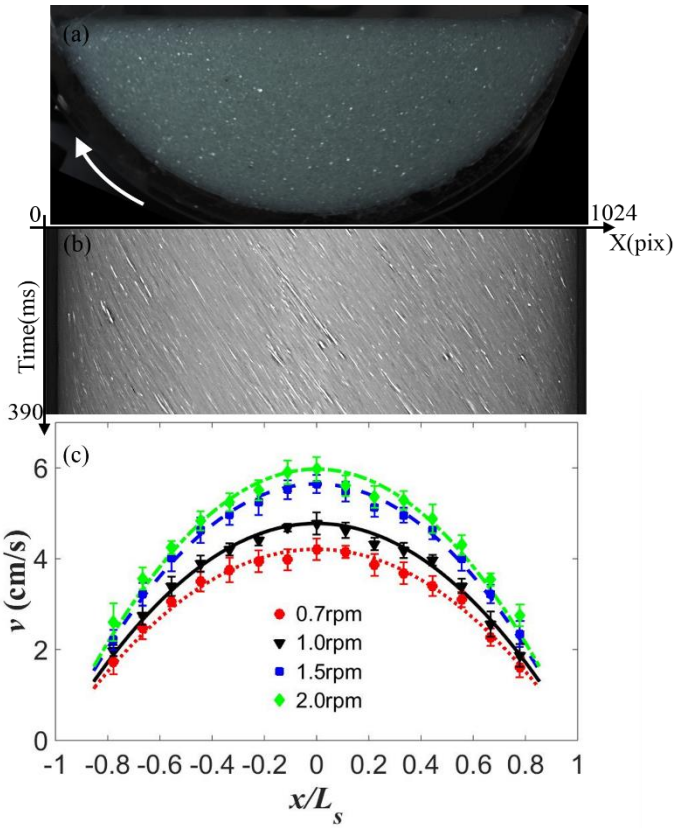

Figure. 5 Measurement results of spherical particles in a 15cm drum. (a) Profile image of the granular bed, which is rotate counterclockwise, in the drum speed of 2 rpm. (b) Original image stack collected by linear CCD over 390 ms. (c) Streamwise velocity profiles at the bed surface for spherical particle at different rotating speeds. The error bars at each data point represent the standard deviation of 10 measurements. The solid line are fitted profiles using Eq 5.

3 Results and discussion

3.1 Primary observation

According to the observation of irregular particles granular flow layer, the shape and velocity distribution of the flow layer are different from the spherical particle flow layer simple model of Khakhar [11]. Figure 6 (a) shows the profile image of the granular materials in the drum, which is not flat like in the case with spherical particles (Figure 5(a)). Thus, the surface can be divided into 3 sections (*i.e.* S1, S2, and S3) along the streamwise direction based on the change of the free surface slope. There are two section with constant slope at the top (S1) and the bottom (S3) with the middle section in between with not constant slope due to formation of a mound. The boundaries of the three

parts are determined by the derivative of the velocity in Figure 6c. We can see that the peaks and valleys of the particle acceleration are in good agreement with the change of the slope of the free surface.

Figure 6 (b) is the composite linear CCD camera image stack of irregular particles which is quite different from the spherical particles case in figure 5 (b). The composite image is not uniform with distinctive difference between sections indicating that the motion of irregular particles is not as uniform like that of spherical particles. While the sections S1 and S3 look similar to each other, the mid-section S2 is looking very different to other two section suggesting that the particle velocity of S1 and S3 is different from that of S2. Figure 6 (c) is the velocity and velocity gradient distribution of the particles in the streamwise direction of granular bed surface measured by SFV method, where the blue line indicates the average particle velocity. Observing the average particle velocity, we can see that the velocity distribution of irregular particles is quite different from that of spherical particles as there are two peaks in the streamwise directions, which are located in the S1 and the S3 segment respectively. This is similar to the irregular limestone particle velocity field measured by Boateng and Barr [18]. We can observe that the particle velocity in S2 is smaller than that of S1 and S3. There is a low point of velocity in S2, corresponding the mound peak position in the centre of the drum free surface.

The red line in figure 6 (c) indicates the derivative of velocity with respect to position. Because the velocity distribution of the flow layer does not change with time, the position of the individual particle can determine the velocity of the particle. The red line indicates the velocity gradient of a particle at this location.

By comparing the velocity v and the velocity gradient $\mathrm{d}v/\mathrm{d}x$, we can see that in the S1 segment, the acceleration of the driving particles speed up, while the resistance increases and the acceleration decreases. When the velocity reaches the first peak, the resistance is larger than the component of gravity in the streamwise direction, and the particle velocity begins to decrease. At the same time, the growth rate of resistance decreases, and resistance reaches the maximum at the boundary between S1 and S2. In S2, the corresponding resistance starts to decrease because the velocity is less than S1, and in the middle of the flow layer, the resistance and the component of gravity reach equilibrium, and the particles velocity reaches the minimum value. Then the particle velocity begins to increase, the resistance decreases and the rate of decrease of the resistance decreases, and the acceleration of speed reaches the maximum at the boundary between S1 and S2. In S3, the particle velocity increases to a maximum and then begins to decrease, and its variation is similar to S1.

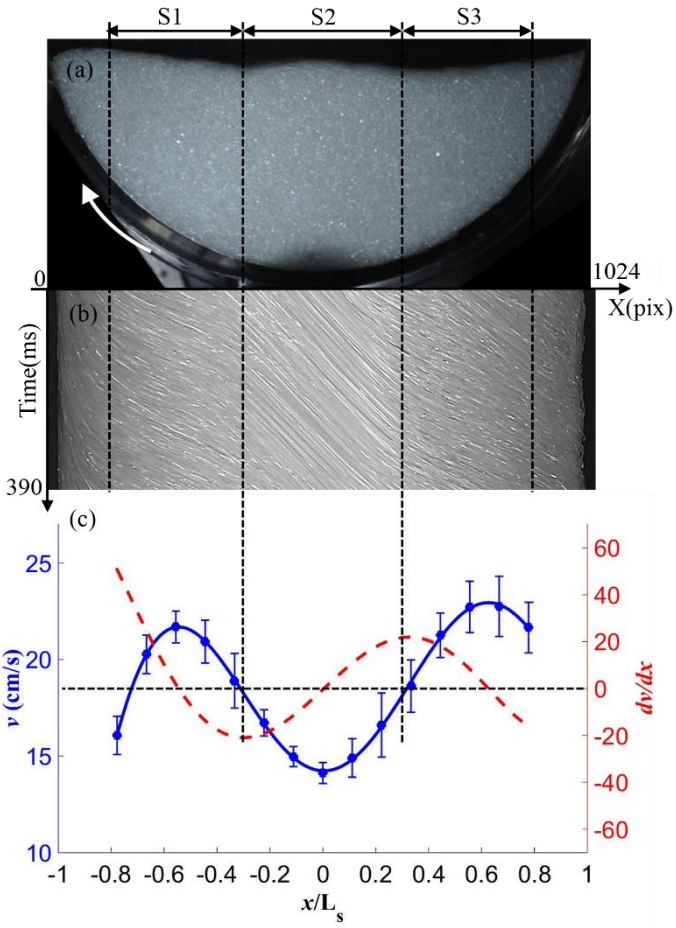

Figure. 6 Measurement results of irregular particles A at a drum rotation speed of 5 rpm. (a) Profile image of the granular bed, which is rotated counterclockwise, in the drum. (b) Original image stack collected by linear CCD and (c) streamwise velocity profile at the bed surface, the error bars at each data point represent the standard deviation of 10 measurements. The blue solid line is obtained by curve fitting. The red line is the derivative of velocity with respect to position.

3.2 Variation of velocity distribution with drum speed

Figure. 7 shows the velocity field distribution of the irregular particle A in the drum at different rotating speed. This experiment shows that as the rotating speed increase, the velocity distribution of irregular particle A can be divided into two distinct regimes. Examples of two regimes profiles are shown in figure 7 (a) and (b). In figure 7 (a), for the drum rotating at 5 rpm, the streamwise velocity profile has two peaks. The first peak r of the velocity profile is smaller than the second peak, but as the rotating speed increase, the first peak gradually increases, while the second peak is almost constant in magnitude. At the same time the magnitude of valley between the two peaks increases with the rotational speed and moves to the right of mid-chord of the profile. Figure 7 (b) shows that after the drum speed increases sufficiently, the middle valley gradually moves to the upper right and merges with the second peak. Consequently, there is only one peak in the velocity profile along streamwise direction of the bed surface, and the irregular particles enter the second regime similar to spherical particles behavior. At lower rotational speeds, the peak is located in the upper half of the particle bed surface and the lower half of the particle bed surface is in a lower velocity state. When the rotational speed increases, the peak point position gradually moving to the upper right. For the drum rotating at 20 rpm, the velocity peak point is near the midpoint of the profile. Figure 7 (c) shows velocity field distribution at 20 rpm which is fitted with Equation (5). In the upper half of the particle flow, the velocity field distribution is in very good agreement with the fitted curve, whereas in the lower half

of the bed surface, the fitted results are larger than the measured velocities. Regarding mound dynamics, at lower rotation speed (up to 7 rpm) the mound has tendency to shift downwards, but at 10 rpm the mound start to expend from the upper half to the lower half and it is very stable. However, at 20 rpm, effect of particle accumulation seems to be weakened, and the mound is not stable, sometimes disappear. This is also illustrated by the 20rpm results in Figure 7(b).

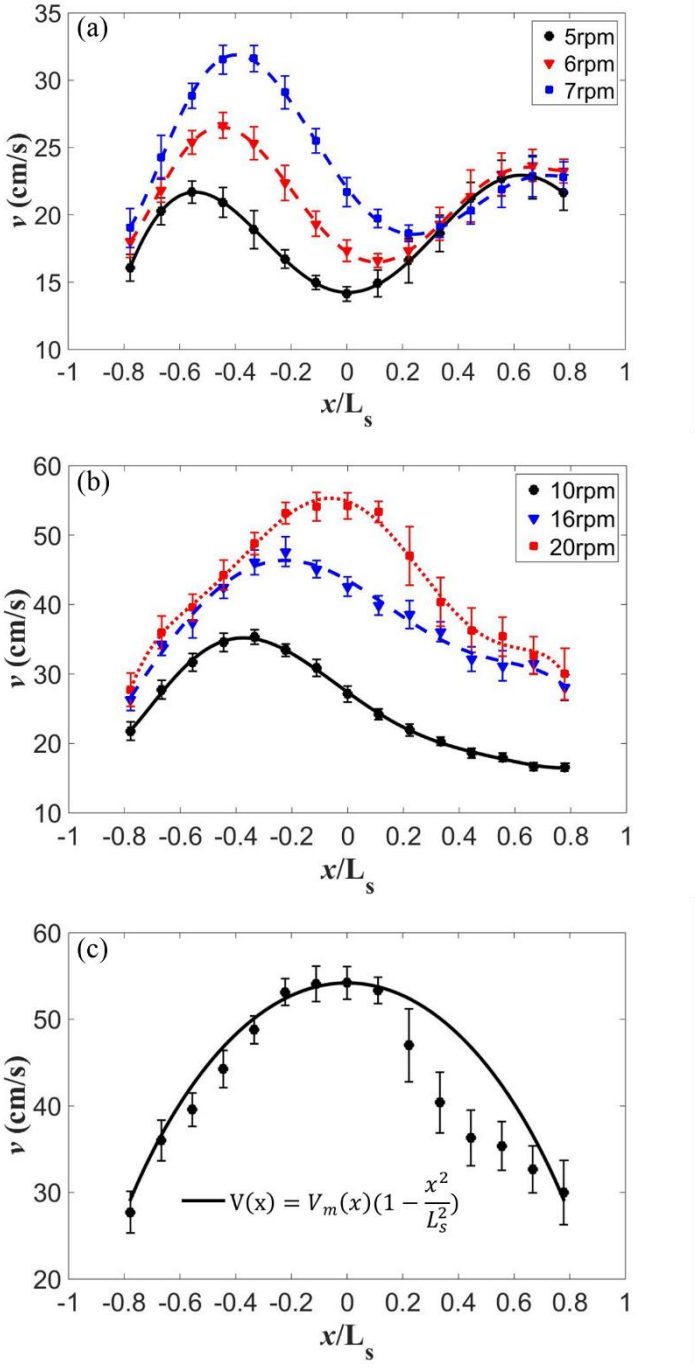

Figure. 7 Streamwise velocity profiles at the bed surface for irregular particle A in two different regimes at lower (a) and higher (b) rotating speeds. The error bars at each data point represent the standard deviation of 10 measurements while the solid line is obtained by curve fitting. (c) Fitting of velocity field distribution at 20 rpm using Equation (5).

3.3 The effect of particle size

Figure. 8(a) is the surface velocity field distribution of larger size irregular particles B at different rotating speeds. The surface of irregular particle B also has two peaks at lower rotating speeds with

corresponding two peaks in velocity profiles. However, as the rotating velocity increases, the phenomenon of the two peaks gradually disappear, and the velocity distribution tends to be symmetric in the mid-chord similarly to particles A's behavior. Yet, there are some difference in velocity profiles of particles A and B at both lower and higher rotational speeds. At low rotational speeds, there are two peaks for both particle A and particle B. However, during the disappearance of two peaks, the peak at the upper part of particle A shifted to the middle position, while the valley at the middle of particle B disappeared gradually. Moreover, although there is accumulation near the middle of particle B, we did not observe a stable and obvious mound like the one in Figure 6 (a).

Figure. 8(b) is a comparison of irregular particles A, B at 5 rpm as representative of the first velocity regime at smaller rotational speeds. Particle B, which has a larger particle size, has a velocity greater than the particle A's velocity but also the peaks and valley are not as pronounced. At the same rotational speed, the smaller particle slows down more strongly. It shows that the friction between large particles is smaller and the fluidity is better. Figure 8 (c) shows the velocity comparison of irregular particles A and B with different particle sizes at 10 rpm. We can see that in the lower half of the particle bed, particle B is faster than particle A, and the two peaks of the irregular particles have disappeared. The rotational speed is smaller for particle B to enter such a uniform, continuous state.

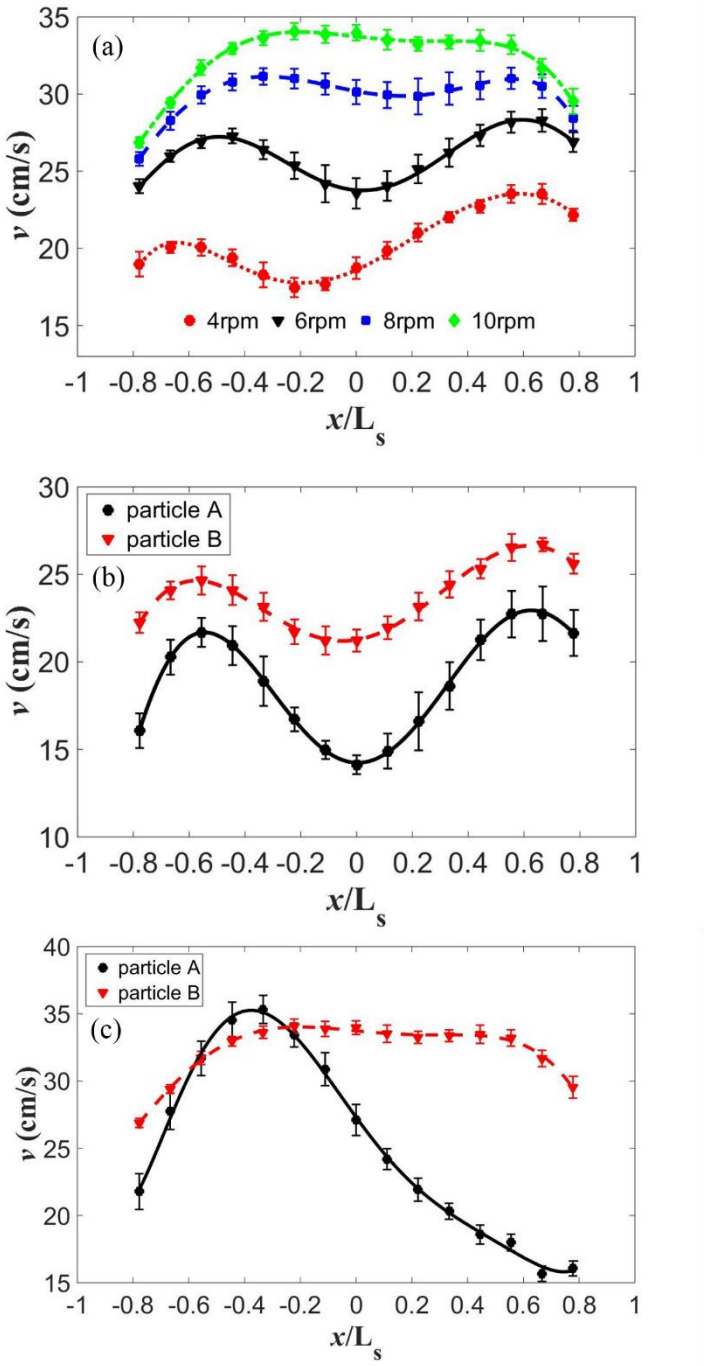

Figure. 8 (a) Streamwise velocity profiles at the bed surface for irregular particle B in a 15 cm drum from 4 rpm to 10 rpm. (b) Streamwise velocity profiles at the bed surface for irregular particle A and B at 5rpm and (c) is at 10 rpm. The error bars at each data point represent the standard deviation of 10 measurements. The solid line which is obtained by curve fitting

3.4 The effect of drum size

Figure 9 shows the velocity distribution of particles B in different diameter drums. The surface velocity of particle B in the 10 cm diameter cylinder is less than that in the larger cylinder, and because of the short flow distance in the drum, the two peak phenomena of irregular particles do not occur. Comparing the results of the 15 cm and 20 cm diameter cylinders, we can see that the speed of particles B within the 20 cm diameter is greater than that within 15 cm and 10 cm, however, the valley speed within the 20 cm cylinder is less than that at 15 cm cylinder. Because the flow distance of the particles in the 20 cm drum is longer, the higher the difference between peak and valley, and the two

peak phenomenon is more obvious.

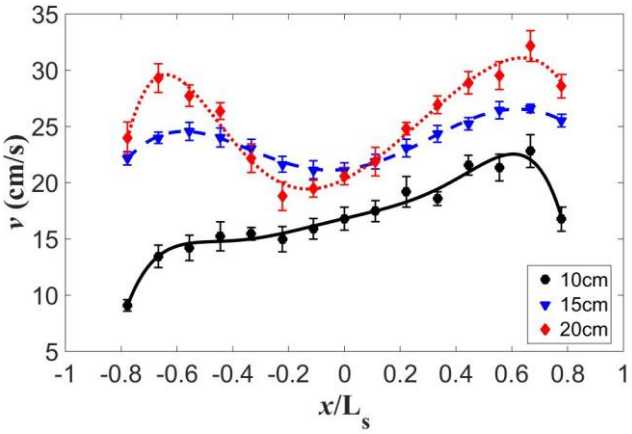

Figure. 9 Particle B surface velocity distribution in different diameter drum at 5rpm, the error bars at each data point represent the standard deviation of 10 measurements. The solid line which is obtained by curve fitting

4 Conclusion

The velocity distribution of irregular particles flow in the drum was studied using SFV technique. Among them, the velocity distribution of irregular particles is significantly different from that of spherical particles. The SFV results show that there is a pile-up process of irregular particles in the rolling mode, and the accumulation is accompanied with deceleration. And this stacking process will change with the drum speed increases. The image of the particle flow clearly shows that the surface of the particle flow of the irregular particles is not a straight line but has a profile change due to packing. Irregular particles in the roll mode, the surface velocity field showed a trough in the middle, while a peak at the top and the bottom. With the increase of the drum speed, the phenomenon of the two peaks in the speed field disappears, and the speed peak exists only in the top part. As the speed continues to increase, the peak gradually shifts right into the middle of the particle bed. This phenomenon of packing appears to be diminished after the size of the irregular particles increases. The results at different roller diameters also show the existence of this build-up. Among them, the larger the diameter of the larger drum, the longer the particles, the accumulation is also more obvious. The SFV proved reliable technique for measurement of surface velocity field in rotating drum, but it also has limitations and can only be used to measure the steady rolling flow of particles. Future work will study two-dimensional particle motion on the surface using SFV measurements based on area array CCDs are needed. The next study will look into measuring velocity field at the side of the drum and also combining it with speckle visibility spectroscopy (SVS) which can measure the fluctuation velocity, so called granular temperature.

Acknowledgements

This work has been supported by the National Natural Science Foundation of China (11572201, 91634202).

Reference

[1] H.M. JAEGER, S.R. NAGEL, Physics of the Granular State, Science (80-.). 255 (1992) 1523–1531.

[2] GDR Midi, On dense granular flows, Eur. Phys. J. E. 14 (2004) 314–365.

[3] G. Seiden, P.J. Thomas, Complexity, segregation, and pattern formation in rotating-drum flows, Rev. Mod. Phys. 83 (2011).

[4] S. Volpato, P. Canu, A.C. Santomaso, Simulation of free surface granular flows in tumblers, Adv. Powder

Technol. 28 (2017) 1028–1037.
[5] J. Mellmann, The transverse motion of solids in rotating cylinders-forms of motion and transition behavior, Powder Technol. 118 (2001) 251–270.
[6] Y.L. Ding, J.P.K. Seville, R. Forster, D.J. Parker, Solids motion in rolling mode rotating drums operated at low to medium rotational speeds, Chem. Eng. Sci. 56 (2001) 1769–1780.
[7] F. Fantozzi, S. Colantoni, P. Bartocci, U. Desideri, Rotary Kiln Slow Pyrolysis for Syngas and Char Production From Biomass and Waste—Part I: Working Envelope of the Reactor, J. Eng. Gas Turbines Power. 129 (2007) 901.
[8] X. Yan Liu, E. Specht, Predicting the fraction of the mixing zone of a rolling bed in rotary kilns, Chem. Eng. Sci. 65 (2010) 3059–3063.
[9] H. Henein, J.K. Brimacombe, A.P. Watkinson, Experimental study of transverse bed motion in rotary kilns, Metall. Trans. B. 14 (1983) 191–205.
[10] R. Li, H. Yang, G. Zheng, Q.C. Sun, Granular avalanches in slumping regime in a 2D rotating drum, Powder Technol. 326 (2018) 322–326.
[11] D. V. Khakhar, J.J. McCarthy, T. Shinbrot, J.M. Ottino, Transverse flow and mixing of granular materials in a rotating cylinder, Phys. Fluids. 9 (1997) 31–43.
[12] D. V. Khakhar, J.J. McCarthy, J.M. Ottino, Radial segregation of granular mixtures in rotating cylinders, Phys. Fluids. 9(1997) 3600-3614.
[13] H.R. Norouzi, R. Zarghami, N. Mostoufi, Insights into the granular flow in rotating drums, Chem. Eng. Res. Des. 102 (2015) 12–25.
[14] O. Dubé, E. Alizadeh, J. Chaouki, F. Bertrand, Dynamics of non-spherical particles in a rotating drum, Chem. Eng. Sci. 101 (2013) 486–502.
[15] D. Suzzi, G. Toschkoff, S. Radl, D. Machold, S.D. Fraser, B.J. Glasser, J.G. Khinast, DEM simulation of continuous tablet coating: Effects of tablet shape and fill level on inter-tablet coating variability, Chem. Eng. Sci. 69 (2012) 107–121.
[16] S. Longo, A. Lamberti, Grain shear flow in a rotating drum, Exp. Fluids. 32 (2002) 313–325.
[17] P. Pandey, R. Turton, Movement of different-shaped particles in a pan-coating device using novel video-imaging techniques, AAPS PharmSciTech. 6 (2005) E237–E244.
[18] M. Engineering, B. Columbia, A.A. Boateng, P. V Barr, Granular flow behaviour in the transverse plane of a partially filled rotating cylinder, J. Fluid Mech. 330 (1997) 233–249.
[19] H. Yang, B.F. Zhang, R. Li, G. Zheng, V. Zivkovic, Particle dynamics in avalanche flow of irregular sand particles in the slumping regime of a rotating drum, Powder Technol. 311 (2017) 439–448.
[20] S. Stanier, J. Dijkstra, D. Leśniewska, J. Hambleton, D. White, D. Muir Wood, Vermiculate artefacts in image analysis of granular materials, Comput. Geotech. 72 (2016) 100–113.
[21] T. Hagemeier, M. Börner, A. Bück, E. Tsotsas, A comparative study on optical techniques for the estimation of granular flow velocities, Chem. Eng. Sci. 131 (2015) 63–75.
[22] Y.C. Chung, S.S. Hsiau, H.H. Liao, J.Y. Ooi, An improved PTV technique to evaluate the velocity field of non-spherical particles, Powder Technol. 202 (2010) 151–161.
[23] A. V. Orpe, D. V. Khakhar, Rheology of surface granular flows, J. Fluid Mech. 571 (2007) 1–32.
[24] T. Hagemeier, C. Roloff, A. Bück, E. Tsotsas, Estimation of particle dynamics in 2-D fluidized beds using particle tracking velocimetry, Particuology. 22 (2015) 39–51.
[25] R. Bandyopadhyay, A.S. Gittings, S.S. Suh, P.K. Dixon, D.J. Durian, Speckle-visibility spectroscopy: A tool to study time-varying dynamics, Rev. Sci. Instrum. 76 (2005).
[26] R. Li, H. Yang, G. Zheng, B.F. Zhang, M.L. Fei, Q.C. Sun, Double speckle-visibility spectroscopy for the dynamics of a passive layer in a rotating drum, Powder Technol. 295 (2016) 167–174.
[27] J.M. Gong, H. Yang, S.H. Lin, R. Li, V. Zivkovic, Spatial filtering velocimetry for surface velocity

measurement of granular flow, Powder Technol. 324 (2018).
[28] T.W. Leadbeater, D.J. Parker, J. Gargiuli, Positron imaging systems for studying particulate, granular and multiphase flows, Particuology. 10 (2012) 146–153.
[29] R. Stannarius, Magnetic resonance imaging of granular materials, Rev. Sci. Instrum. 88 (2017) 51806.
[30] J.T. Ator, Image-Velocity Sensing with Parallel-Slit Reticles, J. Opt. Soc. Am. 53 (1963) 1416.
[31] M.S. Uddin, H. Inaba, Y. Itakura, M. Kasahara, Estimation of the surface velocity of debris flow with computer-based spatial filtering, Appl. Opt. 37 (1998) 6234–6239.
[32] Y. Aizu, T. Asakura, Spatial filtering velocimetry: fundamentals and applications, Springer Series in Optical Science, 116, Springer, 2006.
[33] C. Xu, B. Zhou, D. Yang, G. Tang, S. Wang, Velocity measurement of pneumatically conveyed solid particles using an electrostatic sensor, Meas. Sci. Technol. 19 (2008).
[34] J. Li, C. Xu, S. Wang, Spatial filtering characteristics of electrostatic sensor matrix for local velocity measurement of pneumatically conveyed particles, Meas. J. Int. Meas. Confed. 53 (2014) 194–205.
[35] S. Bergeler, H. Krambeer, Novel optical spatial filtering methods based on two-dimensional photodetector arrays, Meas. Sci. Technol. 15 (2004) 1309–1315.